AD

TECHNICAL REPORT ARBRL-TR-02119

TRACING OF LIGHT RAYS ALONG A PROJECTILE WAKE

R. Sedney
N. Gerber
J. M. Bartos

November 1978

US ARMY ARMAMENT RESEARCH AND DEVELOPMENT COMMAND
BALLISTIC RESEARCH LABORATORY
ABERDEEN PROVING GROUND, MARYLAND

Destroy this report when it is no longer needed.
Do not return it to the originator.

Secondary distribution of this report by originating or sponsoring activity is prohibited.

Additional copies of this report may be obtained from the National Technical Information Service, U.S. Department of Commerce, Springfield, Virginia 22161.

The findings in this report are not to be construed as an official Department of the Army position, unless so designated by other authorized documents.

The use of trade names or manufacturers' names in this report does not constitute indorsement of any commercial product.

REPORT DOCUMENTATION PAGE

READ INSTRUCTIONS BEFORE COMPLETING FORM

1. REPORT NUMBER: TECHNICAL REPORT ARBRL-TR-02119
2. GOVT ACCESSION NO.:
3. RECIPIENT'S CATALOG NUMBER:

4. TITLE (and Subtitle): TRACING OF LIGHT RAYS ALONG A PROJECTILE WAKE

5. TYPE OF REPORT & PERIOD COVERED: Final

6. PERFORMING ORG. REPORT NUMBER:

7. AUTHOR(s):
R. Sedney
N. Gerber
J. M. Bartos

8. CONTRACT OR GRANT NUMBER(s):

9. PERFORMING ORGANIZATION NAME AND ADDRESS:
U.S. Army Ballistic Research Laboratory
(ATTN: DRDAR-BLL)
Aberdeen Proving Ground, Maryland 21005

10. PROGRAM ELEMENT, PROJECT, TASK AREA & WORK UNIT NUMBERS: RDT&E 1L161102AH43

11. CONTROLLING OFFICE NAME AND ADDRESS:
U.S. Army Armament Research & Development Command
U.S. Army Ballistic Research Laboratory
(ATTN: DRDAR-BL)
Aberdeen Proving Ground, Maryland 21005

12. REPORT DATE: NOVEMBER 1978

13. NUMBER OF PAGES: 34

14. MONITORING AGENCY NAME & ADDRESS(if different from Controlling Office):

15. SECURITY CLASS. (of this report): Unclassified

15e. DECLASSIFICATION/DOWNGRADING SCHEDULE:

16. DISTRIBUTION STATEMENT (of this Report)

Approved for public release; distribution unlimited.

17. DISTRIBUTION STATEMENT (of the ebstract entered in Block 20, if different from Report)

18. SUPPLEMENTARY NOTES

19. KEY WORDS (Continue on reverse side if necessary and identify by block number)

Geometrical Optics
Light-Ray Tracing
Miss-Distance Sensor
Projectile Wake
Wake Density Model

20. ABSTRACT (Continue on reverse side if necessary and identify by block number) (1cb)

The propagation of optical radiation longitudinally through the turbulent wake of a supersonic projectile is studied by means of geometrical optics. The differential equations for propagation of light rays in a non-homogeneous medium are integrated numerically for light traveling upstream from a pulsed point source located behind a moving projectile, and the shadow formed on a film located ahead of the projectile is calculated. The index of refraction is obtained from a semi-empirical model for the gas density in the wake. The

(Continued)

20. ABSTRACT (Continued):

calculated magnification of the projectile shadow diameter agrees with measured values to within 5%; such consistency between the calculations and experimental data is taken as justification of the model. This result suggests that geometrical optics is adequate for tracing rays along a wake and, therefore, for performing design calculations in the development of an optical miss distance sensor and design systems for beam rider projectiles and missiles.

TABLE OF CONTENTS

LIST OF ILLUSTRATIONS

LIST OF APPENDIX ILLUSTRATIONS

I. INTRODUCTION

The feasibility of developing an optical miss distance sensor has been investigated recently. Field tests and a wind tunnel test yielded inconclusive results, indicating a need for a better understanding of the optical problems involved. The work reported here addresses this need.

The miss distance sensor can be regarded as a replacement for a tracer round. The general idea is that an optical signal is sent to the projectile, then reflected from the base to a detector. The light source and detector are both located near the gun; consequently, the light will travel primarily through the length of the wake of the projectile. For the analysis of the system it is important to know how the wake affects the light rays, particularly in regard to the strength of the signal received by the detector. A typical mean density distribution in the wake, in the radial direction, shows the lowest density on the axis. From this it can be deduced that the wake should act like a negative lens, tending to diverge the light rays. This qualitative result, first described in Reference 1, was given quantitative meaning by the experiment reported there. Although the method of detecting the effect is not the same in this experiment as in the miss distance sensor, the experiment is important because it provides accurate results in a controlled and convenient manner. The calculations described here are applicable to the miss distance sensor and the experiment, but only application to the latter is discussed. The former will be considered in a separate report.

The experiment produces end-view shadowgraphs of the projectile and wake. The shadow of the projectile appears magnified because it is formed by the diverging light from a near point source and because the wake has a negative lens effect. The experimental set-up is sketched in Figure 1. The light source is pulsed when the projectile is at a distance* $\bar{\ell}$ from the photographic film; this distance is determined accurately by means of a simultaneous side view shadowgraph. The complete projectile shadow does not appear in the end-view shadowgraph because of the hole punctured in the film. A sample result (Case # 1)** is shown in Figure 2; about 60 percent of the circumference is discernible.

---

1. *G. D. Kahl, D. B. Sleator, and D. D. Shear, "Experiments on Wake Optical Properties," Ballistic Research Laboratories Memorandum Report No. 2496, July 1975. AD B005619.*

* Definitions of quantities are given in the List of Symbols section.

** This is the sixth case listed on p. 12 of Reference 1; also, it is Case f listed in Table I on p. 13 of this report.

For miss distance sensors and beam rider projectiles or missiles the wake through which the radiation travels is turbulent, except possibly for a short length near the base. Considerable work has been done on propagation of electromagnetic radiation through a turbulent medium because of applications to the atmosphere; however, the approximations appropriate to that work will generally not apply to a turbulent wake. An important question is whether geometrical or physical optics should be used. The answer depends on the optical system (whether it is diffraction limited or not), the size and shape of the important turbulent eddies (turbulence scale lengths), and the density fluctuations. In this report, rather than justify the geometrical optics approximation a priori, we demonstrate that its predictions compare favorably with experimental results of Reference 1. The additional question arises as to the importance of scattering which can also be treated within the geometrical optics approximation. We calculate only the refractive effects due to mean density variations in the wake; the results of Reference 1 are used to justify neglecting scattering.

The calculation requires that the index of refraction be specified; therefore, the density, using the Dale-Gladstone law. For a turbulent wake the density, ρ, is expressed as

$$\rho = \tilde{\rho} + \rho' \cdot$$

where $\tilde{\rho}$ is the mean density and ρ' is the fluctuating part of ρ. The optical effects of ρ' would be to scatter or diffuse the light; variations in $\tilde{\rho}$ will produce refraction, the only effect considered here.

An axisymmetric wake is assumed in this work. Actually the wake is never axisymmetric, even for a projectile at zero angle of attack. The near wake is usually close to being axisymmetric; but the far wake, i.e., many calibers from the body, can develop oscillations with amplitudes of the order of the wake diameter[2]. The complications of a statistical treatment, even for $\tilde{\rho}$, are not warranted for this study, and the comparisons with results from Reference 1 justify this approach.

II. EQUATIONS

Figure 3 shows a diagram of the coordinate system, the origin being in the center of the projectile base. The ray tracing equations are derived from Fermat's principle, which states that a ray of light will travel between two points along the path for which the time of travel is an extremum. (All lengths have been non-dimensionalized by

---

2. *C. H. Murphy and E. R. Dickinson, "Growth of the Turbulent Wake Behind a Supersonic Sphere," AIAA Journal, Vol. 1, pp. 339-342, February 1963. Also see BRL Memorandum Report No. 1388. AD 280216.*

$\bar{D}$, the diameter of the projectile base; dimensional lengths will be designated with a bar.) For this variational problem the resulting Euler equations[3] are

$$\begin{aligned} \partial F/\partial x - d(\partial F/\partial \dot{x})/dz &= 0 \\ \partial F/\partial y - d(\partial F/\partial \dot{y})/dz &= 0 \end{aligned} \tag{1}$$

where

$$\dot{x} \equiv dx/dz, \qquad \dot{y} \equiv dy/dz$$

$$F(z, x, y, \dot{x}, \dot{y}) \equiv n(x, y, z)\ (\dot{x}^2 + \dot{y}^2 + 1)^{\frac{1}{2}} \tag{2}$$

For an axisymmetric index of refraction field, $n(x, y, z) = n(r, z)$, the equations can be simplified if cylindrical coordinates are used:

$$x = r \cos\theta, \qquad y = r \sin\theta, \qquad z = z \ .$$

In this formulation θ is an ignorable coordinate, in the language of dynamics. Although n is axisymmetric the light rays will be three-dimensional curves in general; these are called skew rays. A ray remains in a plane only if the initial direction is in a plane through the axis; these are called planar rays. It can be shown[4] that a skew ray can be treated as a planar ray if the index n is replaced by

$$m \equiv [n^2 - (h^2/r^2)]^{\frac{1}{2}} \ ,$$

where h is a constant. Specifically, the Euler equation for r(z) is

$$d^2r/dz^2 = [1 + (dr/dz)^2]\ [\partial m/\partial r - (dr/dz)\ (\partial m/\partial z)]/m \tag{3}$$

with $\theta(z)$ determined from the quadrature

$$d\theta/dz = (h/r)\ [1 + (dr/dz)^2]^{\frac{1}{2}}/(n^2r^2 - h^2)^{\frac{1}{2}} \ . \tag{4}$$

The quantity h, constant along a light ray, can be related to the location and direction of the ray at the initial point, $z = z_o$; thus

$$h \equiv n_o r_o^{\,2} (d\theta/dz)_o/[1 + (dr/dz)_o^{\,2} + r_o^{\,2}\ (d\theta/dz)_o^{\,2}]^{\frac{1}{2}} \ .$$

---

3. *M. Born and E. Wolf, Principles of Optics, Pergamon Press, New York, 1959, p. 717.*

4. *R. K. Luneburg, Mathematical Theory of Optics, University of California Press, Berkeley and Los Angeles, 1964, p. 191.*

The Euler equations simplify further for the set of planar rays; for these h = 0 and $d\theta/dz = 0$ from Eq. (4).

The index of refraction, n(z, r), together with its partial derivatives, is provided as input to the calculation.

III. DENSITY DISTRIBUTION MODEL

The index of refraction in the flow field is related linearly to the density of the gas:

$$n = n_\infty + (n_\infty - 1)\ [(\rho/\rho_\infty) - 1] \quad . \tag{5}$$

In this form of the Dale-Gladstone law, the wave length of light enters through n_∞, the ambient index of refraction. A crucial part of the problem is to obtain accurate data for the wake density. A semi-empirical model developed by Finson[5] for the wake density distribution is employed in this work. It has proven satisfactory for the cases studied thus far.

The key to Finson's wake model is the specification of the velocity on the axis. Beyond the rear stagnation point, the mean velocity on the axis can be specified as a nearly universal function of downstream distance, z. This "universal" function is shown in Figure 2 of Reference 5, based on the results of nine experimental investigations. Additional operations are prescribed for the near wake. Conservation of energy can then be used to relate the velocity and temperature on the axis. Approximate radial profiles can be specified for the temperature from similarity arguments. The density field is then obtained with the perfect gas law, with the additional approximation that the pressure is constant, equal to the ambient value. The formulas used to determine density and density gradients are presented in Appendix A. The Finson model is expected to be applicable for $M_\infty \leqslant 5$, for relatively high Reynolds numbers (10^4 - 10^6), and for a wide variety of body shapes.

IV. NUMERICAL SOLUTION

Refraction ahead of the projectile base is neglected, i.e., the light rays travel undeviated from z = 0 to the film with the direction attained at z = 0. This assumption is justified because (1) the

---

5. *M. L. Finson, "Density Distributions in Supersonic Projectile Wakes," PSI TR-66, Physical Sciences, Inc., Woburn, Massachusetts, Ballistic Research Laboratories Contract Purchase Order No. DAAD05-76-M-D111, October 1976.*

distance traversed here by the light ray is small compared to the length of the wake traveled, and (2) the expansion at the edge of the projectile base and the bow shock wave produce opposing deviations.

The objective of the ray tracing calculation is to determine the shadow of the projectile on the film ahead of it. The rays are determined by solving Eqs. (3) and (4), with initial conditions specified by the position of the light source and the slope of a ray emanating from it. A point source on the x-axis is assumed with coordinates $z = z_o$, $r = r_o$, $\theta = 0$. The slope of a ray is identified by $\dot{r}_o$ and $\dot{\theta}_o$ (dr/dz and $d\theta/dz$ at $z = z_o$). The numerical integration, for given $\dot{r}_o$ and $\dot{\theta}_o$, is terminated at $z = 0$. The ray, for which $r = r_b$, $\theta = \theta_b$ at $z = 0$, is extended as a straight line in the direction $\dot{r}_b$, $\dot{\theta}_b$; and its intersection with the screen occurs at

$$x_s = \ell\, r_b\, \dot{\theta}_b \sin\theta_b + (r_b - \ell\, \dot{r}_b) \cos\theta_b$$

$$y_s = (r_b - \ell\, \dot{r}_b) \sin\theta_b - \ell\, r_b\, \dot{\theta}_b \cos\theta_b \quad , \tag{6}$$

where ℓ is distance from the base of the projectile to the screen.

The computations were carried out on a UNIVAC 1108 and a CDC Cyber 76. The integration interval was maintained sufficiently small in the integration of Eqs. (3) and (4) so that the solution was correct at least to four figures.

All but one of the cases treated here apply to a caliber 30 bullet. Although the base diameter is not quite equal to the full cross-sectional diameter of the bullet because of a slight boattail, we take it equal to the latter. We calculate the "shadow" of the bullet as the trace on the film of those rays which touch the base at its circumference; i.e., $r_b = 0.5$. We call these the "grazing rays" and denote them by $\dot{r}_{og}$, $\dot{\theta}_{og}$. A systematic procedure for determining grazing rays is described in Appendix B.

Our choice of shadow-bounding rays is an approximation; some rays touching the base at $r_b = 0.5$ are blocked by the bullet and do not truly constitute grazing rays. This effect is discussed in Section V; it is concluded that the shadow boundary is not seriously affected by this approximation.

V. PLANAR RAYS

Planar rays (mentioned in Section II) are particularly useful; they simplify ray tracing, but results are still informative. Here $\dot{\theta} = \theta = 0$; all light rays are in the x, z plane and are characterized by a single parameter, $\dot{r}_o$, for a fixed light source and screen. The grazing rays, $\dot{r}_{og}$ for $x_b = \pm 0.5$, are easily found from the computed x_b vs $\dot{r}_o$ relationship. These rays produce the two boundary points of the projectile shadow on the x-axis if there is no caustic. Since the shadow of the projectile is approximately a circle on every shadowgraph, the two bounding points of light penetration provide an indication of the size and displacement of the shadow. For these rays the computed magnification of the projectile cross-section is defined as $\Delta x_{mag} \equiv x_{sn} - x_{sf}$, x_{sn} and x_{sf} being the coordinates on the screen of the 'near' and 'far' planar grazing rays, respectively. The 'near' grazing ray is the one on the same side of the shadow as the light source.

For Case # 1 (Figure 2) the two planar grazing rays correspond to (1) $\dot{r}_{og} = 0.00941$ (near ray) and (2) $\dot{r}_{og} = 0.01101$ (far ray). Figure 4 shows these rays; the z scale was compressed in order to exhibit the full ray conveniently. The far grazing ray changes curvature near the z-axis and is concave downward when it strikes the projectile base.

In Table I* we present a comparison of measured and computed magnifications for nine cases. The first eight are those listed on p. 12 of Reference 1. Rounds a through h are caliber 30 bullets; parameters are $\overline{D} = 0.782$ cm, $r_o = 5.754$ projectile diameters, $n_\infty = 1.0002780$, $C_D = 0.316$, $M_\infty = 2.41$, $\gamma = 1.4$, and $T_w/T_\infty = 1.10$. Round i is a spherical projectile; the "base" is taken to be the area of intersection with a plane (normal to the trajectory) through the center of the sphere. Parameters are $\overline{D} = 0.800$ cm, $r_o = 2.063$, $n_\infty = 1.0002780$, $C_D = 0.968$, $M_\infty = 2.81$, $\gamma = 1.4$, and $T_w/T_\infty = 1.00$.

With the exception of Case h, which appears to be out of line in the measurement column, the experimental and theoretical values agree to within 4½%. The close agreement is a little surprising considering the approximation involved in the model, especially for the wake density. The consistency of the data and calculations is taken as justification of the model.

---

* The dashed lines separate the three values of $z + \ell$.

Table I. Measured and Computed Magnifications

Case	$z_o + \ell$	ℓ	Meas. Magnif.	Δx_{mag}
a	259.9	13.54	1.140	1.108
b	259.9	15.17	1.175	1.121
c	646.4	14.68	1.150	1.119
d	646.4	26.34	1.230	1.213
e	646.4	30.50	1.260	1.246
f	646.4	52.85	1.410	1.420
g	646.4	75.13	1.640	1.603
h	646.4	90.95	1.630	1.721
i	148.2	31.84	1.366	1.373

A parameter study was carried out corresponding to an experiment where the light source and screen are fixed, but the timing of the light pulse is varied; thus r_o and $z_o + \ell$ are fixed. The values are those of Cases c through h in Table I. Figure 5 shows how the magnification, Δx_{mag}, changes with location of the projectile and illustrates strikingly the lens effect of the wake by comparing the wake flow and no flow magnifications. It is noteworthy that the wake flow Δx_{mag} varies linearly with ℓ over a wide range of ℓ.

Part of the light striking the base at its edge on the near side is blocked by the projectile so that a portion of the edge of the shadow is formed by rays other than those passing through $r_b = 0.5$. An estimate based on planar rays can be made of the deviation of our computed shadow from that formed by the true grazing rays on the near side. We assume that the projectile is a cylinder of length k having a blunt nose so that the actual near grazing ray (planar) passes through $r = 0.5$ at the front end of the cylinder. Then the corrected shadow coordinate $x_s = (x_{sn})_i$ can be obtained in two steps:

(1) find $\dot{r}_{oi}$, the value of $\dot{r}_o$ for which

$$r_b - k\,\dot{r}_b = 0.5 \quad ,$$

and designate the corresponding r_b by r_{bi};

(2) evaluate $(x_{sn})_i$ from

$$(x_{sn})_i = r_{bi} - (\ell/k)\,(r_{bi} - 0.5) \quad .$$

For a length k = 5, the "corrected" magnifications exceed the original values by no more than 1½% in Cases d through h in Table I. This result suggests that neglect of blocked rays does not produce serious errors.

An inspection of the data was made to determine whether any non-blocked light rays fell inside the trace of the grazing rays on the screen. This occurrence would denote the presence of a caustic. No caustic was found in any of the cases studied.

VI. SHADOW OF PROJECTILE

The shadow of the projectile is bounded by the locus of the incident grazing rays on the screen. Figure 6 shows the calculated shadow for Case No. 1. Also shown are the location of the projectile in the x, y plane and the no-flow image produced by the point source. The latter is a circle given by

$$[x_s + (r_o \ell/z_o)]^2 + y_s^2 = (1/4)\,[1 + (\ell/z_o)]^2 \quad , \tag{7}$$

where the subscript s denotes the coordinate value on the screen. The diagram shows that the wake has appreciably enlarged the shadow beyond the simple geometrical projection, or no-flow image. The image is symmetrical about the x-axis because the point source is located on the axis. Although it is not a circle, it is only slightly eccentric, the height being larger than the width by approximately 3½%.

Figure 6 provides the theoretical picture to be compared with the shadowgraph of Figure 2. The projectile shadow in Figure 2 does not appear clearly symmetrical about any axis. This lack of symmetry is probably caused by an unsymmetrical wake and the yawing of the bullet. Other shadowgraphs do, however, exhibit more pronounced symmetry.

The calculation predicts two effects of the wake; namely, (1) magnification of the object, discussed in Section V, and (2) displacement of its image to the left. The displacement is more difficult to measure because it additionally requires locating the line of fire. Displacement was measured for only one of the rounds listed in Table I of Section V; namely, for the spherical projectile, Round i. The

measured displacement of the center of the circle was 0.509 calibers while the computed value was 0.525 diameters.

An additional comparison of measured and computed horizontal magnifications was made; in this case the projectile was a sphere. The grazing rays were taken to be those which intersected the circle formed by the sphere and the plane (normal to the trajectory) through its center. The two results disagreed by less than one percent.

VII. CONCLUDING REMARKS

On the basis of results reported here and in Reference 1, it appears feasible to make optical measurements in ballistic experiments in which light traverses the wake of a projectile. Furthermore, it seems possible to predict the paths of light rays with reasonable accuracy on the basis of geometrical optics and theoretical models for wake flow. The model presented here is verified by experimental results and, therefore, can be used with confidence in performing design calculations in the development of miss distance sensors and beam rider projectiles and missiles.

ACKNOWLEDGEMENT

The authors are grateful to Mr. G. D. Kahl for supplying the experimental data used here. They also appreciate especially the insight he provided in many helpful discussions.

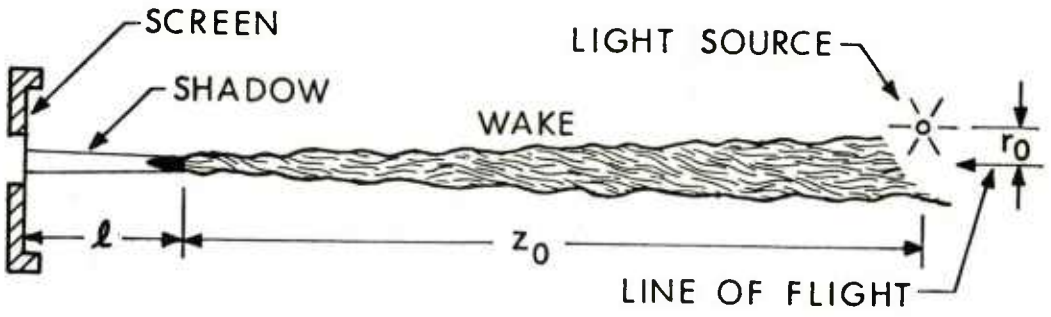

Figure 1. Physical Setup of Experiment

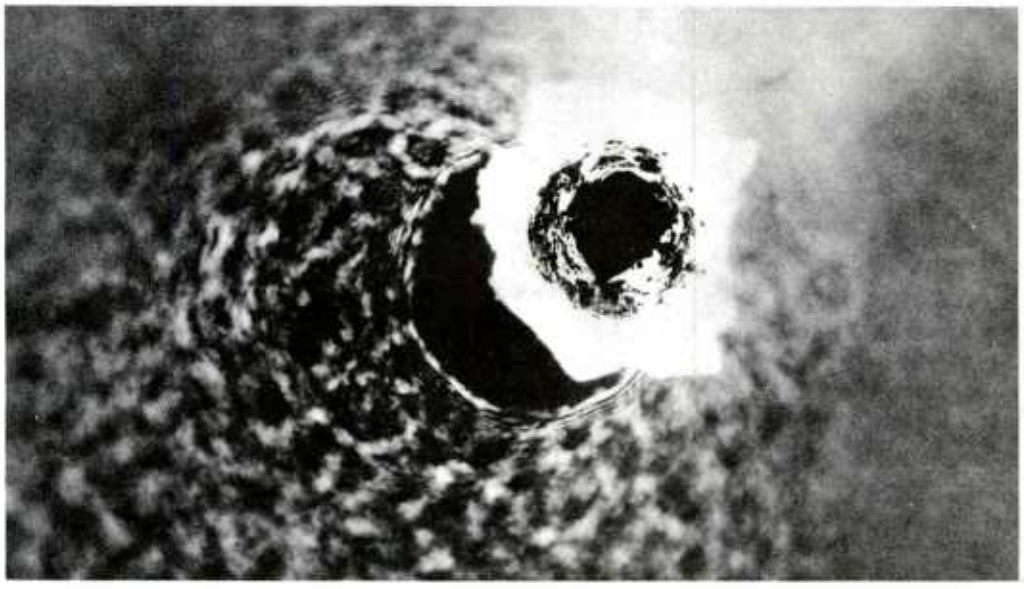

Figure 2. End-On Shadowgraph of Projectile -- Case No. 1
($\overline{D}$ = 0.782 cm, $\overline{\ell}$ = 41 cm, $\overline{z}_o$ = 464 cm,
$\overline{r}_o$ = 4.5 cm, M_∞ = 2.41, C_D = 0.316)

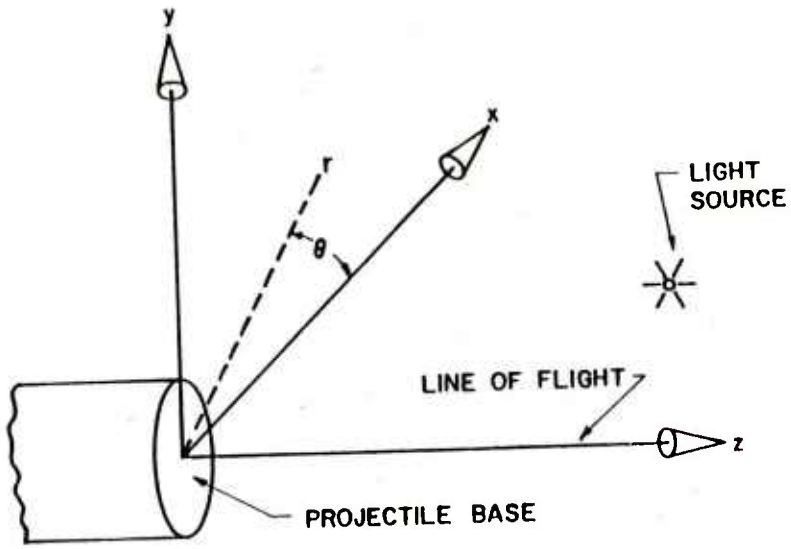

Figure 3. Coordinate System

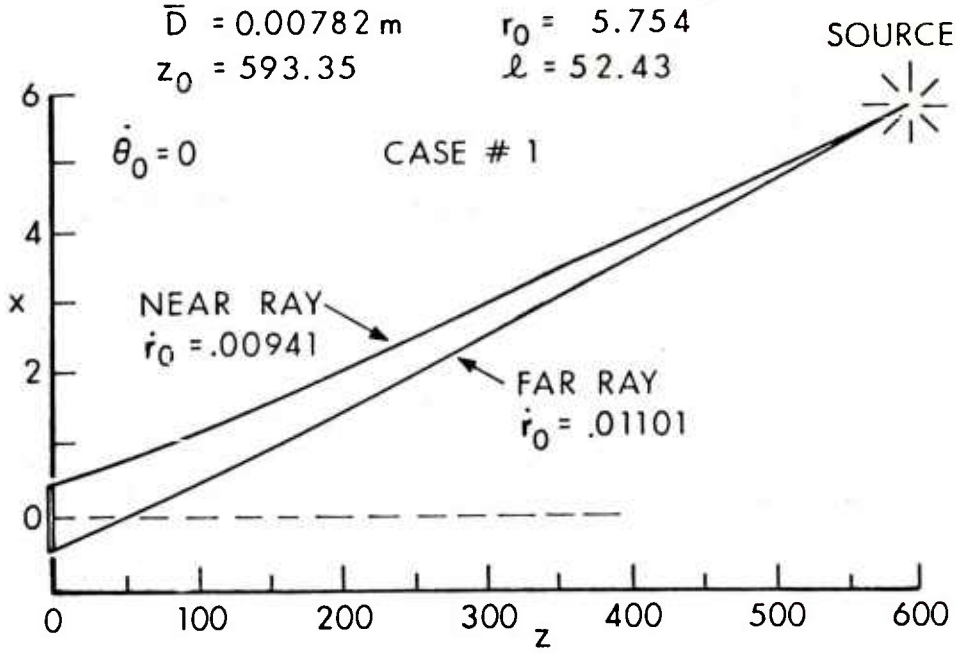

Figure 4. Planar Grazing Rays -- Case No. 1

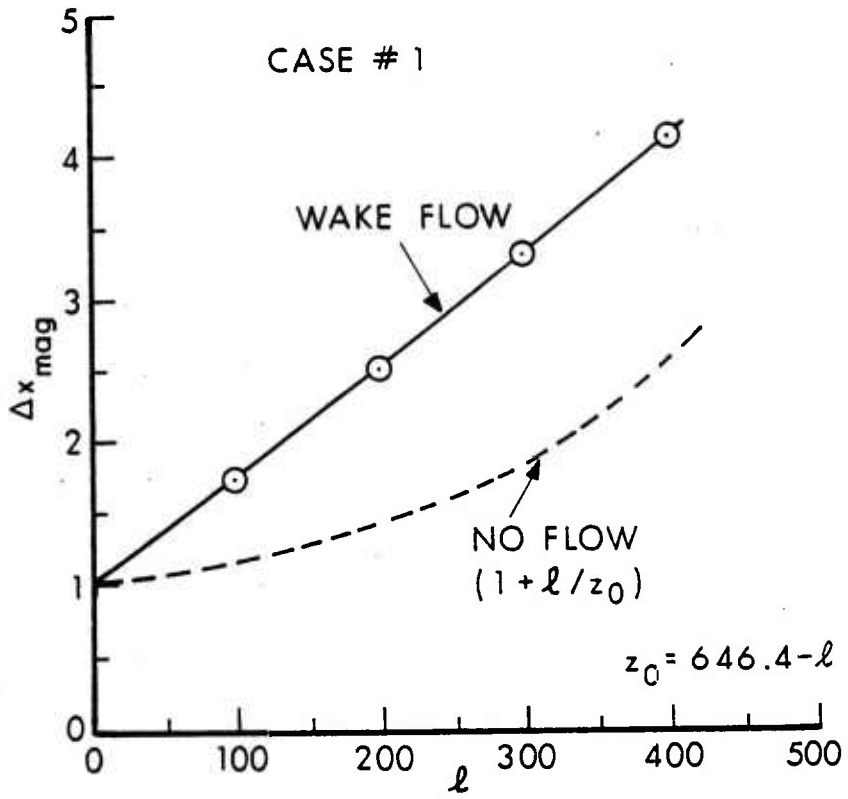

Figure 5. Magnification of Projectile Base as a Function of Location of Projectile (Light Source and Screen Locations Fixed) -- Case No. 1

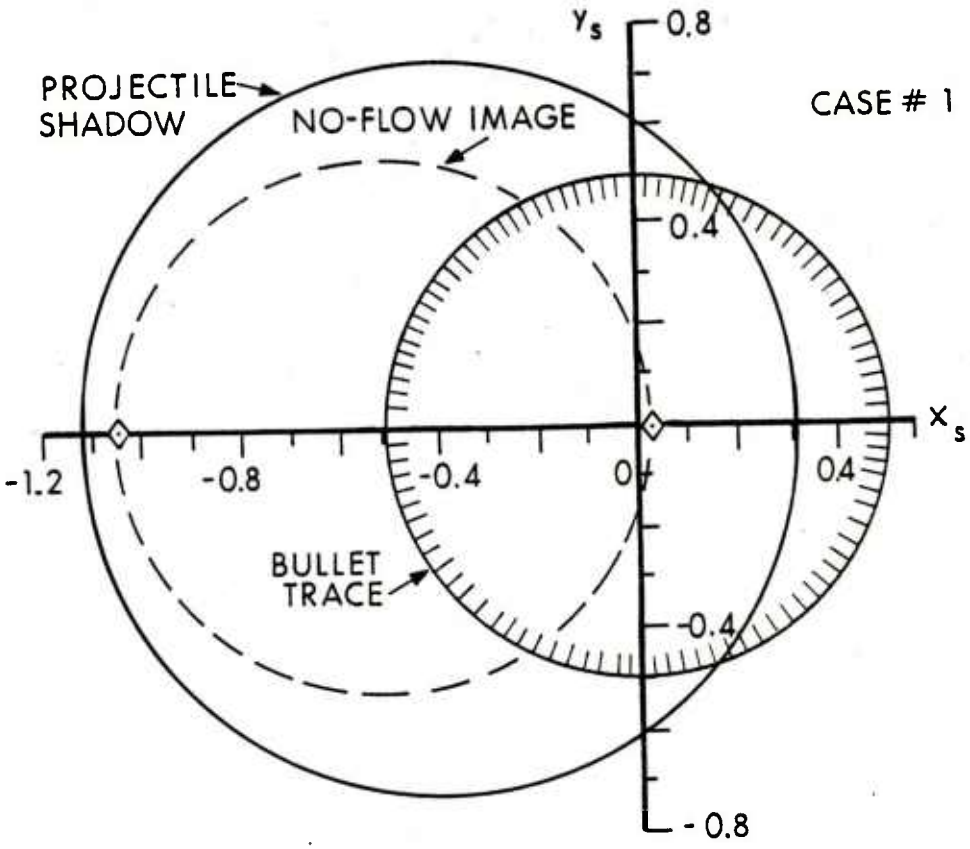

Figure 6. Calculated End-On Shadow of Projectile -- Case No. 1

REFERENCES

1. G. D. Kahl, D. B. Sleator, and D. D. Shear, "Experiments on Wake Optical Properties," Ballistic Research Laboratories Memorandum Report No. 2496, July 1975. AD B005619.

2. C. H. Murphy and E. R. Dickinson, "Growth of the Turbulent Wake Behind a Supersonic Sphere," *AIAA Journal*, Vol. 1, pp. 339-342, February 1963. Also, BRL Memorandum Report No. 1388. AD 280216.

3. M. Born and E. Wolf, Principles of Optics, Pergamon Press, New York, 1959, p. 717.

4. R. K. Luneburg, Mathematical Theory of Optics, University of California Press, Berkeley and Los Angeles, 1964, p. 191.

5. M. L. Finson, "Density Distributions in Supersonic Projectile Wakes," PSI TR-66, Physical Sciences, Inc., Woburn, Massachusetts; Ballistic Research Laboratories Contract Purchase Order No. DAAD05-76-M-D111, October 1976.

LIST OF SYMBOLS

Dimensional lengths are designated by a super bar; otherwise lengths, including coordinates, are non-dimensionalized by $\overline{D}$.

C_D	projectile drag coefficient
$\overline{D}$	diameter of projectile base
F	integrand in extremum integral -- Eqs. (1) and (2)
h	constant on a three-dimensional light ray -- Eq. (3) et seq.
H	total enthalpy of air
k	length of cylindrical portion of projectile
ℓ	distance between base of projectile and downrange screen
m	equivalent refractive index in planar ray equation for non-planar rays (Section II)
M_∞	flight Mach number of projectile
n	index of refraction of air in flow field
n_∞	ambient index of refraction of air (= 1.0002780)
r, θ	cylindrical polar coordinates (θ in radians) -- Figure 3
$\dot{r}_{og}$, $\dot{\theta}_{og}$	initial values of $\dot{r}$ and $\dot{\theta}$ for grazing rays
T	temperature
T_W	an average temperature of projectile wall
T_∞	ambient temperature
u	mean axial velocity component relative to projectile
x_s, y_s	x, y of a point on the film
x_{sn}, x_{sf}	values x_s for near and far planar grazing rays, respectively
x, y, z	rectangular coordinates -- Figure 3

Δx_{mag}	($\equiv x_{sn} - x_{sf}$) magnification of projectile base
γ	ratio of specific heats of air (= 1.4)
ρ	flow field density of air

Subscripts

o	$z = z_o$ -- plane of light source (initial value of variables)
b	z = 0 -- plane of projectile base
$c\ell$	r = 0 -- center line
g	grazing rays (for which $r_b = 0.5$)
i	planar rays grazing the front end of cylinder
s	plane of film (screen) -- $z = -\ell$
∞	free stream, or ambient, conditions

Superscripts

.	= d/dz
—	dimensional length

APPENDIX A: REFRACTIVE INDEX IN THE WAKE

The following quantities are assumed known: M_∞, C_D, γ, n_∞, and T_w/T_∞. The index of refraction, $n(r,z)$, in the flow field behind the projectile, described in Reference 5, is obtained from the formulas which now follow, evaluated in sequence.

The formulae for computing the velocity deficit are given in Eqs. (A.1)-(A.13). The velocity deficit, $\overset{*}{u}$, expressed as $\overset{*}{u} = \overset{*}{u}_1 + \overset{*}{u}_2$, where $\overset{*}{u}_1$ is an analytical approximation to the empirical curve for $\Delta u_o/u_\infty$ in Figure 2 of Reference 5, and $\overset{*}{u}_2$ is an approximation to the curve in Figure 3 of Reference 5.

$\overset{*}{u} \equiv (u_\infty - u_{c\ell})/u_\infty$ -- definition, where u is mean axial velocity component relative to projectile

$$\overset{*}{z} = z\,(1.1284/C_D^{\frac{1}{2}}) , \qquad dz/d\overset{*}{z} = 0.88623\, C_D^{\frac{1}{2}} \tag{A.1}$$

$$\text{If} \quad 0 \leqslant \overset{*}{z} < 1 , \qquad \overset{*}{u}_1 = 0.5 , \qquad d\overset{*}{u}_1/d\overset{*}{z} = 0 \tag{A.2}$$

$$\text{If} \quad 1 \leqslant \overset{*}{z} < 13.0 , \qquad \overset{*}{u}_1 = \tfrac{1}{2} \exp\,[-0.072662\,(\ln \overset{*}{z})^2]$$
$$d\overset{*}{u}_1/d\overset{*}{z} = -0.14532\, \overset{*}{u}_1\, (\ln \overset{*}{z})/\overset{*}{z} \tag{A.3}$$

$$\text{If} \quad 13.0 \leqslant \overset{*}{z} \leqslant 1{,}000.0 , \qquad \overset{*}{u}_1 = 2.3561\, \overset{*}{z}^{-0.79073}$$
$$d\overset{*}{u}_1/d\overset{*}{z} = -0.79073\, \overset{*}{u}_1/\overset{*}{z} \tag{A.4}$$

$$\text{If} \quad 1{,}000.0 < \overset{*}{z} , \qquad \overset{*}{u}_1 = \overset{*}{z}^{-2/3}$$
$$d\overset{*}{u}_1/d\overset{*}{z} = -\,(2/3)\, \overset{*}{u}_1/\overset{*}{z} \tag{A.5}$$

$$q = z - \tfrac{1}{2} \tag{A.6}$$

$$\text{If} \quad q < 0.0 , \qquad \overset{*}{u}_2 = 0.50 , \qquad d\overset{*}{u}_2/d\overset{*}{z} = 0.0 \tag{A.7}$$

$$\text{If} \quad 0.0 \leqslant q < 0.060 , \qquad \overset{*}{u}_2 = 0.50 - (13/3)\, q$$
$$d\overset{*}{u}_2/d\overset{*}{z} = -\,(13/3)\, dz/d\overset{*}{z} \tag{A.8}$$

If $0.06 \leqslant q < 0.340$,

$$\overset{*}{u}_2 = 0.34083 - 1.8761\ q + 3.2618\ q^2 \qquad (A.9)$$

$$d\overset{*}{u}_2/d\overset{*}{z} = [-\ 1.8761 + 6.5236\ q]\ dz/d\overset{*}{z}$$

If $0.340 \leqslant q < 0.671$,

$$\overset{*}{u}_2 = 0.12109 - 0.12085\ q \qquad (A.10)$$

$$d\overset{*}{u}_2/d\overset{*}{z} = -\ 0.12085\ dz/d\overset{*}{z}$$

If $0.671 \leqslant q < 1.321$,

$$\overset{*}{u}_2 = 0.081292 - 0.061539\ q \qquad (A.11)$$

$$d\overset{*}{u}_2/d\overset{*}{z} = -\ 0.061539\ dz/d\overset{*}{z}$$

If $1.321 \leqslant q$, $\quad \overset{*}{u}_2 = 0$, $\quad d\overset{*}{u}_2/d\overset{*}{z} = 0 \qquad (A.12)$

$$\overset{*}{u} = \overset{*}{u}_1 + \overset{*}{u}_2 , \qquad d\overset{*}{u}/d\overset{*}{z} = d\overset{*}{u}_1/d\overset{*}{z} + d\overset{*}{u}_2/d\overset{*}{z} \qquad (A.13)$$

The relation between velocity deficit and temperature is developed in Eqs. (A.14)-(A.18). Eq. (A.18) is Eq. (2) of Reference 5. The centerline deficit in total enthalpy, $\Delta\overset{*}{H}$ in Eq. (A.17), is small for the applications of this model to projectile flight. We have derived a different, presumably more accurate, expression for it; viz,

$$\Delta\overset{*}{H} = 0.0136\ R_w^{\,2}\ (2\overline{d}/\overline{D})\ [1 - (T_w/T_\infty)\ N_\infty^{\,-1}] ,$$

where $\overline{d}$ is an effective heat transfer body length, approximately equal to, but less than, the actual body length.

$\Delta\overset{*}{H} \equiv (H_\infty - H_{c\ell})/H_\infty$ -- definition where H is total enthalpy and $\tilde{h}$ is enthalpy: $H \equiv \tilde{h} + u^2/2$.

$\overset{*}{T} \equiv T_{c\ell}/T_\infty$ -- definition

If $z < 0.5$,

$$R^2 = 26.514\ C_D^{\,-2/3}\ r^2$$

$$R_w \equiv R\ (r = \tfrac{1}{2})$$

$$R_w^{\,2} = 6.6285\ C_D^{\,-2/3} \qquad (A.14)$$

$$dR_w^{\,2}/dz = 0$$

If $0.5 \leqslant z$,

$$R^2 = 16.703\ r^2\ (C_D\ z)^{-2/3}$$

$$R_w^{\,2} = 4.1758\ (C_D\ z)^{-2/3} \tag{A.15}$$

$$dR_w^{\,2}/dz = -(2/3)\ R_w^{\,2}/z$$

$$N_\infty = 1 + \tfrac{1}{2}\ (\gamma - 1)\ M_\infty^{\,2} \tag{A.16}$$

$$\overset{*}{\Delta H} = 4 \times 10^{-3}\ R_w^{\,2}\ [1 - (T_w/T_\infty)\ N_\infty^{\,-1}] \tag{A.17}$$

$$\overset{*}{T} = 1 + \tfrac{1}{2}\ (\gamma - 1)\ M_\infty^{\,2}\ (2 - \overset{*}{u})\ \overset{*}{u} - N_\infty \overset{*}{\Delta H} \tag{A.18}$$

The σ that is obtained from Eq. (A.19) is the η of Eq. (5) in Reference 5. This is a density-transformed radius, depending both on r and z. Eq. (A.22) results from the assumption of a Gaussian radial profile of temperature with respect to σ, the perfect gas law, and the assumption of constant pressure.

Now solve the following functional equation for σ:

$$F\ (\sigma) \equiv \sigma + 2.941\ (\overset{*}{T} - 1)\ [1 - \exp\ (-0.34\ \sigma)] - R^2 = 0 \tag{A.19}$$

This equation is solved by the method of false position; the following two initial guesses σ_1 and σ_2 have proven successful in generating a convergent sequence of approximations:

$$\sigma_1 = R^2 - 2.941\ (\overset{*}{T} - 1)\ , \qquad \sigma_2 = R^2/\overset{*}{T} \tag{A.20}$$

$$E = \exp\ (-0.34\ \sigma) \tag{A.21}$$

$$\rho/\rho_\infty = 1/[1 + (\overset{*}{T} - 1)\ E] \tag{A.22}$$

$$n = n_\infty + (n_\infty - 1)\ [(\rho/\rho_\infty) - 1] \tag{A.23}$$

$$\partial\ (\rho/\rho_\infty)/\partial r = 0.68\ (R^2/r)\ (\rho/\rho_\infty)^3\ (\overset{*}{T} - 1)\ E \tag{A.24}$$

$$d\ (\overset{*}{\Delta H})/dz = 4 \times 10^{-3}\ [1 - (T_w/T_\infty)\ N_\infty^{\,-1}]\ dR_w^{\,2}/dz \tag{A.25}$$

$$Q = (\gamma - 1)\ M_\infty^{\,2}\ (1 - \overset{*}{u})\ d\overset{*}{u}/d\overset{*}{z} \tag{A.26}$$

$$d\overset{*}{T}/dz = 1.1284\ C_D^{\,-\frac{1}{2}}\ Q - N_\infty\ d\ (\overset{*}{\Delta H})/dz \tag{A.27}$$

$$\partial\,(\rho/\rho_\infty)/\partial z = -\,(\rho/\rho_\infty)^2\,E\,[1 + (\overset{*}{T} - 1)\,(1 - E)\,(\rho/\rho_\infty)]\,d\overset{*}{T}/dz \qquad (A.28)$$

$$\partial n/\partial r = (n_\infty - 1)\,\partial\,(\rho/\rho_\infty)/\partial r \qquad (A.29)$$

$$\partial n/\partial z = (n_\infty - 1)\,\partial\,(\rho/\rho_\infty)/\partial z \qquad (A.30)$$

$$h \equiv h\,(r_o,\ z_o,\ \dot{r}_o,\ \dot{\theta}_o) \equiv n_o r_o^{\,2}\dot{\theta}_o/[1 + \dot{r}_o^{\,2} + r_o^{\,2}\dot{\theta}_o^{\,2}]^{\frac{1}{2}}\ ,$$

where n_o is evaluated from Eq. (A.23) for r_o, z_o the very first time this sequence of formulas is used. (See Eq. (4), et seq.)

$$m = [n^2 - (h/r)^2]^{\frac{1}{2}} \qquad (A.31)$$

$$\partial m/\partial z = (n/m)\,\partial n/\partial z \qquad (A.32)$$

$$\partial m/\partial r = (1/m)\,[n\,\partial n/\partial r + (h^2/r^3)] \qquad (A.33)$$

APPENDIX B: DETERMINATION OF GRAZING RAYS

For a given firing, $r_b = r_b(\dot{r}_o, \dot{\theta}_o)$, and the locus of grazing rays in the $\dot{r}_o$, $\dot{\theta}_o$ plane must be found numerically. The usual procedure is to take a fixed value, say, of $\dot{\theta}_o$, then compute r_b for a range of $\dot{r}_o$ and pick that value of $\dot{r}_o$ for which $r_b = 0.5$. Reasonable estimates for $\dot{r}_{og}$ and $\dot{\theta}_{og}$ can be found beforehand, as shown below.

A very useful aid is a plot of the $\dot{r}_{og}$, $\dot{\theta}_{og}$ grazing ray locus for the no-flow condition, namely for the straight lines between the light source and the boundary of the projectile base. The equation is

$$\dot{\theta}_{og}^2 = [(1/4) - (r_o - \dot{r}_{og} z_o)^2]/(r_o z_o)^2 \quad .$$

This curve is shown in Figure B.1 for Case No. 1.

The appropriate $\dot{r}_{og}$, $\dot{\theta}_{og}$ curve can be obtained easily, e.g., for a succession of points moving gradually away from the planar values of $\dot{r}_{og}$. For a given $\dot{\theta}_o$ the range of $\dot{r}_o$ to be searched can be estimated in advance (Figure B.1). As an example, in Figure B.1, for $\dot{\theta}_o = 0.2 \times 10^{-4}$ the two dashed horizontal segments represent reasonable search ranges for $\dot{r}_{og}$. In other areas it will be more appropriate to fix $\dot{r}_{og}$ and search for $\dot{\theta}_{og}$, as for example, at $\dot{r}_{og} = 0.0100$.

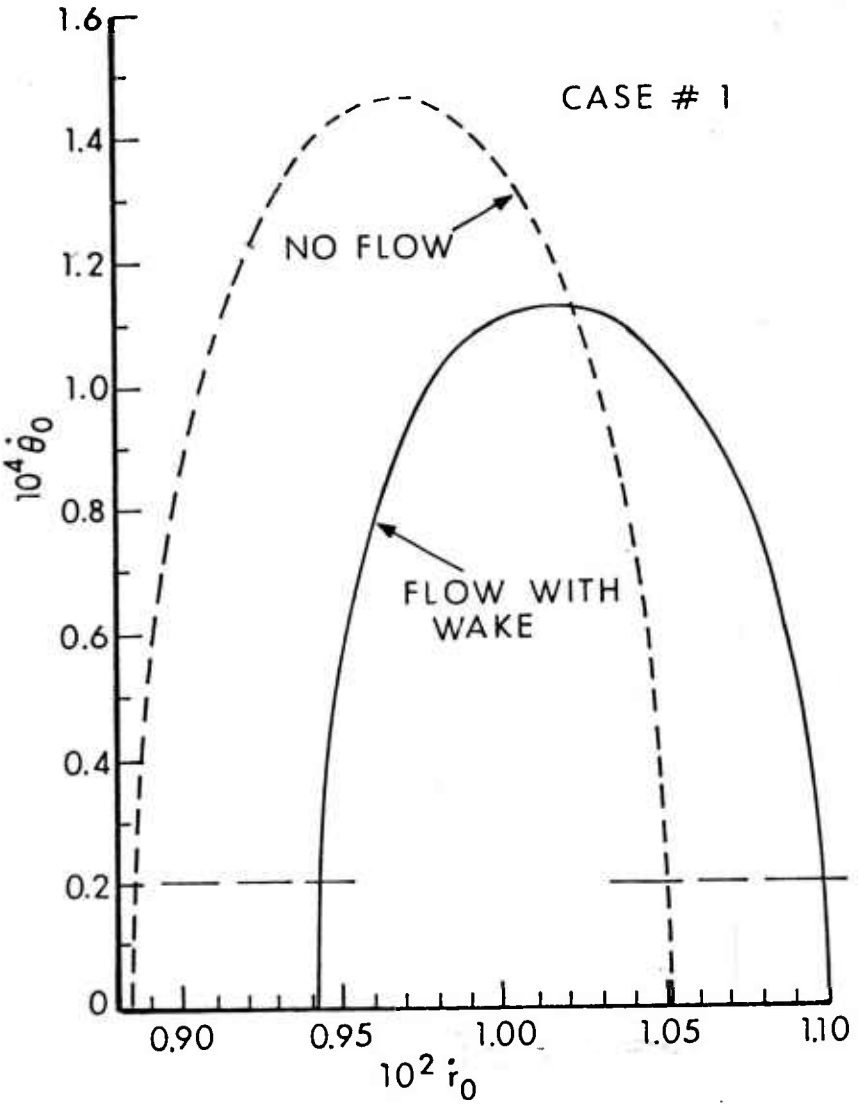

Figure B.1. Locus of Grazing Rays in $\dot{r}_o$, $\dot{\theta}_o$ Plane -- Case No. 1

DISTRIBUTION LIST

No. of Copies	Organization
12	Commander Defense Documentation Center ATTN: DDC-TCA Cameron Station Alexandria, VA 22314
1	Commander US Army Materiel Development and Readiness Command ATTN: DRCDMD-ST, N. Klein 5001 Eisenhower Avenue Alexandria, VA 22333
1	Commander US Army Aviation Research and Development Command ATTN: DRSAV-E P. O. Box 209 St. Louis, MO 63166
2	Director US Army Air Mobility Research and Development Laboratory ATTN: SAVDL-D, W.J. McCroskey Ames Research Center Moffett Field, CA 94035
1	Commander US Army Electronics Research and Development Command Technical Support Activity ATTN: DELSD-L Fort Monmouth, NJ 07703
1	Commander US Army Communications Research & Development Cmd ATTN: DRDCO-PPA-SA Fort Monmouth, NJ 07703
1	Commander US Army Jefferson Proving Ground ATTN: STEJP-TD-D Madison, IN 47250
2	Commander US Army Missile Research and Development Command ATTN: DRDMI-R DRDMI-TD, Mr. R. Deep Redstone Arsenal, AL 35809
1	Commander US Army Missile Research and Development Command Advanced System Concepts Office ATTN: COL Cranford Redstone Arsenal, AL 35809
1	Commander US Army Missile Materiel Readiness Command ATTN: DRSMI-AOM Redstone Arsenal, AL 35809
1	Commander US Army Tank Automotive Research & Development Cmd ATTN: DRDTA-UL Warren, MI 48090
3	Commander US Army Armament Research and Development Command ATTN: DRDAR-TSS (2 cys) DRDAR-LCA-F, A. Loeb Dover, NJ 07801
1	Commander US Army Armament Materiel Readiness Command ATTN: DRSAR-LEP-L, Tech Lib Rock Island, IL 61299
1	Director US Army TRADOC Systems Analysis Activity ATTN: ATAA-SL, Tech Lib White Sands Missile Range NM 88002

DISTRIBUTION LIST

No. of Copies	Organization
1	Commander US Army Research Office ATTN: Dr. R. E. Singleton P. O. Box 12211 Research Triangle Park NC 27709
1	Commander US Army Waterways Experiment Station ATTN: R. H. Malter Vicksburg, MS 39180
1	Commander US Army Harry Diamond Laboratories ATTN: Branch 420, H. Davis 2800 Powder Mill Road Adelphi, MD 20783
1	Commander US Army Natick Research and Development Command ATTN: DRXRE, Dr. D. Sieling Natick, MA 01762
1	AGARD-NATO ATTN: R. H. Korkegi APO New York 09777
1	Director US Army Advanced BMD Technology Center P. O. Box 1500 Huntsville, AL 35809
1	Commander US Army Ballistic Missile Defense Systems Command Huntsville, AL 35804
3	Commander US Naval Air Systems Command ATTN: AIR-604 Washington, DC 20360
3	Commander Naval Ordnance Systems Command ATTN: ORD-0632 ORD-035 ORD-5524 Washington, DC 20360
2	Commander David W. Taylor Naval Ship Research & Development Cmd ATTN: H. J. Lugt, Code 1802 S. de los Santos, Head High Speed Aero Div. Bethesda, MD 20084
3	Commander Naval Surface Weapons Center ATTN: Code GX, Dr. G. Moore F. H. Maille Code DX-21, Lib Br. Dahlgren, VA 22448
5	Commander Naval Surface Weapons Center Applied Aerodynamics Division ATTN: K. R. Enkenhus M. Climent S. M. Hastings A. E. Winklemann W. C. Ragsdale Silver Spring, MD 20910
1	Commander Naval Weapons Center ATTN: Code 233, Info Sci Div China Lake, CA 93555
3	Director Naval Research Laboratory ATTN: Tech Info Div Code 7700, D.A. Kolb Code 7720, Dr. E.McClean Washington, DC 20390
2	ADTC (ADBPS-12) Eglin AFB, FL 32542

DISTRIBUTION LIST

No. of Copies	Organization
1	AFATL (DLDL, Dr. D.C. Daniel) Eglin AFB, FL 32542
1	AFWL (DEV) Kirtland AFB, NM 87117
2	AFFDL (W.L.Hankey; J.S. Shang) Wright-Patterson AFB, OH 45433
4	Director National Aeronautics and Space Administration ATTN: D. R. Chapman J. Rakich W. C. Rose B. Wick Ames Research Center Moffett Field, CA 94035
2	Director National Aeronautics and Space Administration George C. Marshall Space Flight Center ATTN: MS-I, Lib R-AERO-AE, Mr. A. Felix Huntsville, AL 35812
1	Director Jet Propulsion Laboratory ATTN: Tech Library 4800 Oak Grove Drive Pasadena, CA 91103
5	Director National Aeronautics and Space Administration ATTN: J. E. Carter E. Price J. South J. R. Sterrett Tech Library Langley Research Center Langley Station Hampton, VA 23365
1	Director National Aeronautics and Space Administration Lewis Research Center ATTN: MS 60-3, Tech Lib 21000 Brookpark Road Cleveland, OH 44135
3	Aerospace Corporation ATTN: T. D. Taylor H. Mirels R. L. Varwig Aerophysics Lab P. O. Box 92957 Los Angeles, CA 90009
3	ARO, Inc. ATTN: J. D. Whitfield R. K. Matthews J. C. Adams Arnold AFB, TN 37389
1	AVCO Systems Division ATTN: B. Reeves 201 Lowell Street Wilmington, MA 01887
2	The Boeing Company Commercial Airplane Group ATTN: W. A. Bissell, Jr. M. S. 1W-82, Org 6-8340 P. E. Rubbert Seattle, WA 98124
2	Calspan Corporation ATTN: A. Ritter M. S. Holden P. O. Box 235 Buffalo, NY 14221
1	General Dynamics ATTN: Research Lib 2246 P. O. Box 748 Fort Worth, TX 76101

DISTRIBUTION LIST

No. of Copies	Organization
2	General Electric Company, RESD ATTN: R. E. Melnik L. G. Kaufman Research Department Bethpage, NY 11714
2	Lockheed-Georgia Company ATTN: B. H. Little, Jr. G. A. Pounds Dept. 72074, Zone 403 86 South Cobb Drive Marietta, GA 30062
1	Lockheed Missiles and Space Company ATTN: Tech Info Center 3251 Hanover Street Palo Alto, CA 94304
4	Martin-Marietta Laboratories ATTN: S. H. Maslen S. C. Traugott K. C. Wang H. Obremski 1450 S. Rolling Road Baltimore, MD 21227
2	McDonnell Douglas Astronautics Corporation ATTN: J. Xerikos H. Tang 5301 Bolsa Avenue Huntington Beach, CA 92647
1	McDonnell-Douglas Corporation Douglas Aircraft Company ATTN: T. Cebeci 3855 Lakewood Boulevard Long Beach, CA 90801
1	Northrup Corporation Aircraft Division ATTN: S. Powers 3901 W. Broadway Hawthorne, CA 90250
1	Physical Sciences, Inc. ATTN: M. L. Finson Woburn, MA 01801
2	Sandia Laboratories ATTN: F. G. Blottner Tech Lib Albuquerque, NM 87115
2	United Aircraft Corporation Research Laboratories ATTN: M. J. Werle Library East Hartford, CT 06108
1	Vought Systems Division LTV Aerospace Corporation ATTN: J. M. Cooksey Chief, Gas Dynamics Lab, 2-53700 P. O. Box 5907 Dallas, TX 75222
2	California Institute of Technology ATTN: Tech Library D. Coles Aeronautics Dept. Pasadena, CA 91109
1	Cornell University Graduate School of Aero Engr ATTN: Library Ithaca, NY 14850
2	Illinois Insitute of Technology ATTN: M. V. Morkovin H. M. Nagib 3300 South Federal Chicago, IL 60616

DISTRIBUTION LIST

No. of Copies	Organization
1	The Johns Hopkins University ATTN: S. Corrsin, Dept. of Mechanics & Materials Science Baltimore, MD 21218
1	Louisiana State University Department of Physics ATTN: R. G. Hussey Baton Rouge, LA 70803
2	Massachusetts Institute of Technology ATTN: E. Covert Tech Library 77 Massachusetts Avenue Cambridge, MA 02139
2	North Carolina State University Mechanical and Aerospace Engineering Department ATTN: F. F. DeJarnette J. C. Williams Raleigh, NC 27607
1	Notre Dame University ATTN: T. J. Mueller Dept. of Aero Engr South Bend, IN 46556
2	Ohio State University Dept. of Aeronautical and Astronautical Engineering ATTN: S. L. Petrie O. R. Burggraf Columbus, OH 43210
3	Princeton University James Forrestal Research Ctr Gas Dynamics Laboratory ATTN: S. M. Bogdonoff S. I. Cheng Tech Library Princeton, NJ 08540
1	Purdue University Thermal Science & Prop Center ATTN: Tech Library W. Lafayette, IN 47907
1	Rutgers University Department of Mechanical, Industrial, and Aerospace Engineering ATTN: R. H. Page New Brunswick, NJ 08903
1	Southern Methodist University Department of Civil and Mechanical Engineering ATTN: R. L. Simpson Dallas, TX 75275
1	Southwest Research Institute Applied Mechanics Reviews 8500 Culebra Road San Antonio, TX 78228
1	University of California-Davis ATTN: Prof. H. A. Dwyer Davis, CA 95616
2	University of California-San Diego Department of Aerospace Engineering and Mechanical Engineering Sciences ATTN: P. Libby Tech Library La Jolla, CA 92037
1	University of Cincinnati Department of Aerospace Engineering ATTN: R. T. Davis Cincinnati, OH 45221

DISTRIBUTION LIST

No. of Copies	Organization
1	University of Colorado Department of Astro-Geophysics ATTN: E. R. Benton Boulder, CO 80302
2	University of Maryland ATTN: W. Melnik J. D. Anderson College Park, MD 20740
2	University of Mighigan Dept of Aeronautical Engineering ATTN: W. W. Wilmarth Tech Library East Engineering Building Ann Arbor, MI 48104
1	University of Santa Clara Department of Physics ATTN: R. Greeley Santa Clara, CA 95053
1	University of Texas Department of Aerospace Engr. ATTN: J. C. Westkaemper Austin, TX 78712
1	University of Virginia Dept of Aerospace Engineering and Engineering Physics ATTN: I. D. Jacobson Charlottesville, VA 22904
1	University of Washington Dept of Mechanical Engineering ATTN: Tech Library Seattle, WA 98195
1	University of Wyoming ATTN: D. L. Boyer University Station Laramie, WY 82071
1	Virginia Polytechnic Institute Dept of Aerospace Engineering ATTN: G. R. Inger Blacksburg, VA 24061
1	Woods Hole Oceanographic Institute ATTN: J. A. Whitehead Woods Hole, MA 02543

Aberdeen Proving Ground

Dir, USAMSAA
Cdr, USATECOM
ATTN: DRSTE-SG-H
Cdr/Dir, USA CSL, EA
ATTN: Munitions Sys Div
Bldg. 3330
E. A. Jeffers
W. C. Dee
W. J. Pribyl
Armament Concepts Ofc
Bldg. 3516 (DRDAR-ACW)
M. C. Miller